IEEE Access
Multidisciplinary ⋮ Rapid Review ⋮ Open Access Journal

Received 9 November 2023, accepted 26 November 2023, date of publication 30 November 2023,
date of current version 6 December 2023.

Digital Object Identifier 10.1109/ACCESS.2023.3337829

RESEARCH ARTICLE

Experimental Validation of Second-Order Adaptive Fuzzy Logic Controller for Grid-Connected DFIG Wind Power Plant

BASEM E. ELNAGHI[1], M. N. ABELWHAB[1], FATHY EL SAYED AHMED ABDEL-KADER[2], AHMED M. ISMAIEL[1], REHAM H. MOHAMMED[3], AND MOHAMED E. DESSOUKI[4]

[1]Electrical Power and Machines Department, Faculty of Engineering, Suez Canal University, Ismailia 41522, Egypt
[2]Electrical Power and Machine Department, Faculty of Engineering, Menoufia University, Shebeen El-Kom 32611, Egypt
[3]Electrical Computer and Control Engineering Department, Faculty of Engineering, Suez Canal University, Ismailia 41522, Egypt
[4]Electrical Engineering Department, Faculty of Engineering, Port Said University, Port Said 42523, Egypt

Corresponding author: Mohamed E. Dessouki (dessouky_m@yahoo.com)

ABSTRACT This paper introduces a second-order adaptive fuzzy logic controller (SO-AFLC) to enhance the characteristics of a doubly fed induction generator (DFIG) inside a grid-tied wind power plant (WPP). SO-AFLCs were utilized to maximize the output of the DFIG wind power plant (WPP) and improve dynamic responsiveness with extremely low mean square error. When comparing the mean square error of SO-AFLC with proportional-integral controllers (PI) and adaptive fuzzy logic controllers (AFLC), the reductions are 87.38% and 40.39%, respectively. This controller prevents overshoots and oscillations. DFIG wind power plant is modeled and simulated using Matlab/Simulink package. Under the unit step wind speed profile, SO-AFLC improved the steady-state error in the Cp waveform by 63.25% compared with the PI controller and 13.12% compared with AFLC. DSpace1104 is used to conduct an experimental investigation to validate the simulation results. In addition, realistic data from the wind farm at RAS Ghareb in the Gulf of Suez, Egypt, are used in this study to achieve more realistic results. Compared to those obtained with PI and AFLC, the results obtained using SO-AFLCs showed fast time response, high convergence rate, reduced peak overshoot, less undershoot, and low steady-state error in terms of power coefficient of the turbine, DC link voltage control, and rotor speed tracking. In addition, a wind turbine performance index based on gross system integral absolute error (IAE) is provided. This index is used to illustrate the SO-AFLC methodology's viability compared to AFLC and PI under the same wind turbine conditions.

INDEX TERMS SO-AFLC, DFIG, MPPT, wind energy.

I. INTRODUCTION

Due to the exhaustion of conventional fossil fuels, renewable energy resources will be more in demand as alternatives. Wind energy can be considered a leading technology for clean energy because of its low environmental impact, competitive pricing, and efficiency. Since wind turbines were connected to the grid, power electronic converters have been employed, and this technology has developed [1], [2], [3]. Numerous wind generators, such as doubly fed induction generators (DFIG) and permanent magnet synchronous generators (PMSG), work best with wind turbines. The manufacturing of permanent magnet (PM) machines is still challenging because of the expensive nature of PM and its demagnetization at high temperatures. However, DFIGs are incorporated into many wind turbines. Despite its complicated design, it has several benefits over other kinds of wind turbine generators [4]. The DFIG-based wind turbine's key benefit is that its wide speed range is 20 to 30% above or below the synchronous speed. As a result, only

The associate editor coordinating the review of this manuscript and approving it for publication was Ton Duc Do.

around 20–30% of the stator's rated power can be handled by the converter [5], [6]. The DFIG wind power plant requires six regulators to control the MPPT, DC link voltage, reactive power, and rotor speed.

For modern wind turbines, MPPT should be achieved to benefit from the wind speed. There are numerous methods to achieve MPPT for WPP, such as power signal feedback (PSF), optimum torque (OT), and optimum tip speed ratio (OTSR) [7], [8], [9]. The OT method aims to adjust the torque of the generator to the optimum torque for peak power at any wind speed. The goal is to keep the optimum torque of the generator. This method is fast, efficient, and simple. However, the absence of wind speed measurement is an inherent drawback. Therefore, the reference signal does not directly represent the change in wind speed [10], [11], [12], [13]. PSF employs a closed power control loop which depends on the maximum power curve which depends on pre-known information of WPP. Maximum power curve changes based on the wind turbine [6], [12], [14], [15]. OTSR control provides an efficient technique to capture the greatest mechanical power extraction from WPP. OTSR is commonly used for maximum power harvesting in wind turbine systems because it reduces noise levels and centrifugal forces on the blades. Therefore, OTSR control is employed in this study because of its simplicity and high productivity in quickly varying atmospheric circumstances compared to other control strategies [6], [10], [11]. OTSR requires a speed sensor which increases the cost. So, wind speed estimation (WSE) is introduced in [6]. This method uses complex polynomial approximation equations, which also reduces the system accuracy [6], [9], [10]. The operation of a variable wind speed turbine is illustrated in Fig.1 [16]. The operation can be divided into four zones. Zone 1 is when the speed of the wind is less than cut in speed so the WPP is unable to generate power. Zone 2 is called the MPPT operation zone at which the electromagnetic torque is controlled and the pitch angle is held constant to extract maximum power from WPP. Zone 3 is called the pitch control zone at which the pitch angle is regulated to maintain a constant power. Zone 4 is at which the wind speed is too high so the turbine shuts down using the emergency mechanism [11], [16], [17]. This article is concerned with Zone 2 where MPPT is applicable. The Proportional-integral (PI) controllers are frequently implemented in commercial appliances because of a variety of benefits, including low

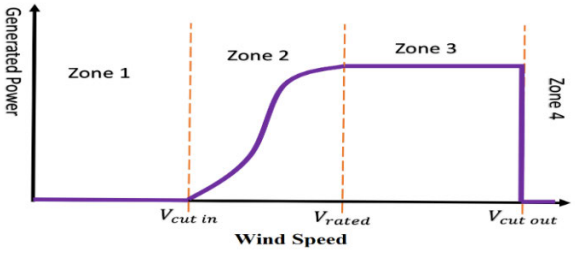

FIGURE 1. Wind speed curve.

adjusting parameters, system durability, a simple construction, and a wide range of stability margins [12]. The system becomes unstable due to the PI controllers' sensitivity to the system's nonlinearity and variable variation [18], [19], [20]. Compared to the PI controllers, AFLC for PI is crucial in aiding in the resolution of these problems. AFLC is used to increase the integrated control system's volatility. Fuzzy logic controllers are used in the design of AFLC to optimize PI's input [14], [21], [22]. AFLCs have advantages that are inherent to them, such as how they handle uncertainty in systems, and their simple architecture. AFLC also has better power tracking performance when compared to PI and normal fuzzy logic controllers [14].

Authors in [23] discuss the design and implementation of a direct power synergetic-sliding mode technique for a doubly-fed induction generator integrated into a variable speed dual-rotor wind power system. The paper also mentions that the direct active and reactive powers control method is widely used in the field of wind power generation and provides better results and ease of implementation compared to other methods. In [24], sliding mode control (SMC) aims to reduce undulations in reactive power, current, torque, and active power. It replaces hysteresis comparators and switching tables with a synergetic-sliding mode command and PWM technique, resulting in better performance and simplicity of implementation compared to other methods. The authors in [25] present that the SMC approach outperforms the H_∞ control in terms of minimizing power undulations caused by wind speed variations and uncertainties. The study highlights the effectiveness of the sliding mode control technique in wind turbine control systems. In [14], the authors investigated the AFLC to adjust MPPT only using Matlab/Simulink and Dspace 1104. The authors in [26] discuss the application of a second-order sliding mode control (SO-SMC) and fuzzy logic control in optimizing energy management in a wind turbine system with battery storage. In [27], the authors propose a direct AFLC that adjusts the generator torque and blade pitch angle to optimize power extraction from the wind. The proposed strategy is evaluated through simulation studies to enhance the characteristics of variable-speed wind turbines (VSWT).

This paper suggested an improvement to AFLC by adding a SO-SMC to AFLC. The SO-SMC is active during the system's transient state. This new control strategy is named SO-AFLC. The results of using SO-AFLCs revealed fast time response, and minimal steady-state error compared to those achieved with PI, and AFLC in terms of power coefficient of the turbine, DC link voltage control, and rotor speed tracking. To the best of our knowledge, the SO-AFLC has not been covered in any literature on wind power plants. This article proposes a sufficient and applicable control system that depends on SO-AFLC. The essential contributions of this research are illustrated as follows:

1) The DFIG wind power plant is investigated through both simulation using Matlab/Simulink 2023a and

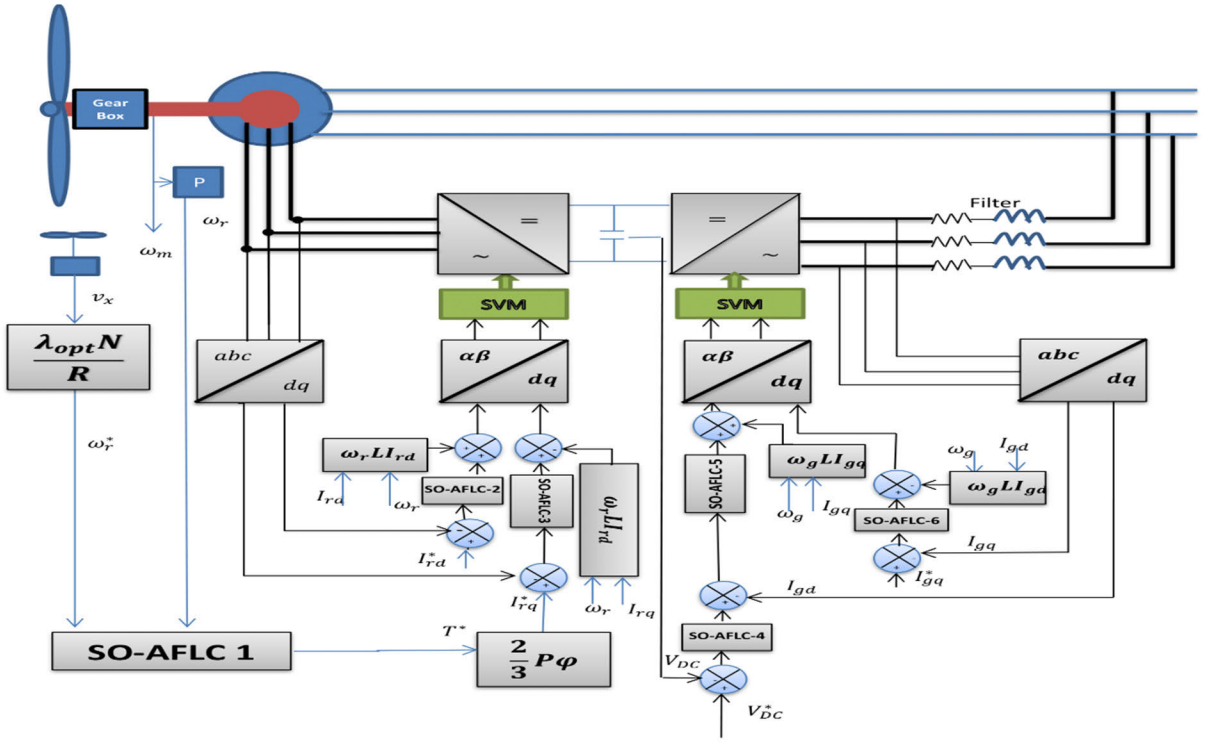

FIGURE 2. The DFIG wind turbine control scheme.

experiment using Dspace 1104 to show the robustness of SO-AFLCs against AFLCs, and PIs.

2) To show the viability of the SO-AFLC methodology against AFLCs, and PIs techniques, a wind turbine performance index based on the gross system integral absolute error (IAE) is provided under identical wind turbine conditions.
3) The system is experimented under measured data from the Ras Ghareb wind farm in Egypt, to produce genuine responses based on actual wind speed data to validate the enhancement of SO-AFLCs against AFLCs, and PIs.

The remainder of this paper is organized as follows. Section I introduces the introduction and Literature reviews. Section II discusses the configuration of the model. In section III, the simulation results are discussed. Section IV explains the operation of the DS 1104 control board. Section V discusses the experimental results using DS 1104. Lastly, the conclusions are presented in Section VI.

II. WIND TURBINE CONFIGURATION

Tip speed ratio control topology for grid-tied DFIG wind power plant is illustrated in Fig.2. The system is formed by DFIG, variable speed wind turbine (VSWT), grid side converter (GSC), rotor side converter (RSC) and link capacitor. The RSC is used to achieve MPPT. GSC is tasked to regulate DC link voltage, and reactive power.

A. MECHANICAL VSWT MODEL

The aerodynamic power out of VSWT (P_m) is expressed as follows [6]:

$$P_m = \frac{1}{2}\rho A v_w^3 C_p(\beta, \lambda) \tag{1}$$

where ρ is the density of air, v_w is the speed of the wind, λ is the tip speed ratio (TSR), $C_P(\beta, \lambda)$ is the power coefficient, β is defined as the pitch angle of the blades.

Here is how the C_p value is formulated [6]:

$$C_p(\beta, \lambda) = D_1\left\{\frac{D_2}{\lambda_i} - D_3\beta - D_4\right\}e^{\frac{D_6}{\lambda_i}} + D_5\lambda \tag{2}$$

$$\lambda = \frac{\omega R}{v_w} \tag{3}$$

$$\frac{1}{\lambda_i} = \frac{1}{\lambda + 0.08\beta} - \frac{0.035}{\beta^3 + 1} \tag{4}$$

where R is the radius of the blade, the wind turbine constants D_1 to D_6 are: $D_1 = 0.5176, D_2 = 116, D_3 = 0.4$, $D_4 = 5, D_5 = 0.0068$, and $D_6 = -21$;

The C_p and λ relation is shown at various pitch angles (β), as illustrated in Fig. 3. To guarantee maximum power value, the turbine must operate at optimum value for C_p, which should coincide with the ideal tip speed ratio (λ_{opt}).

At $\beta = 0$, $\lambda_{opt} = 8.1$, and $C_{p_{max}} = 0.48$, The power reaches its maximum value, according to WT specifications. So, the highest amount of electric power is reached at these values as obtained from Fig. 3.

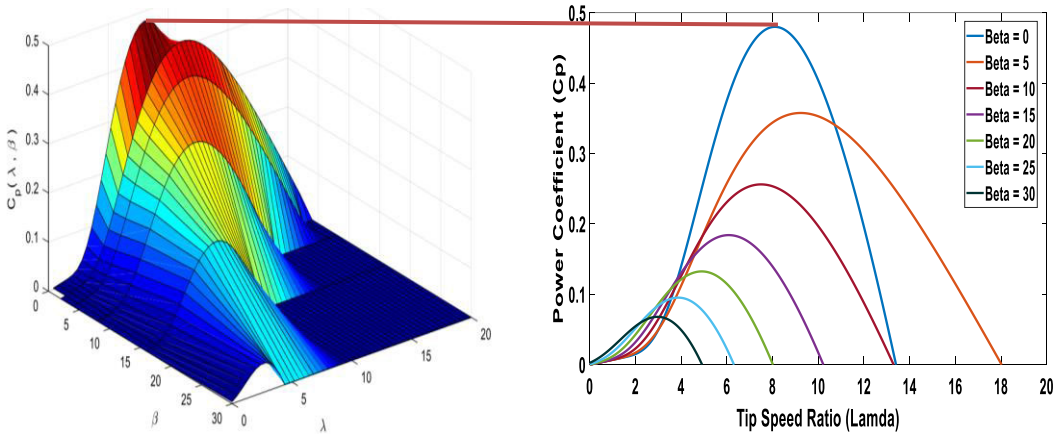

FIGURE 3. The wind turbine characteristics.

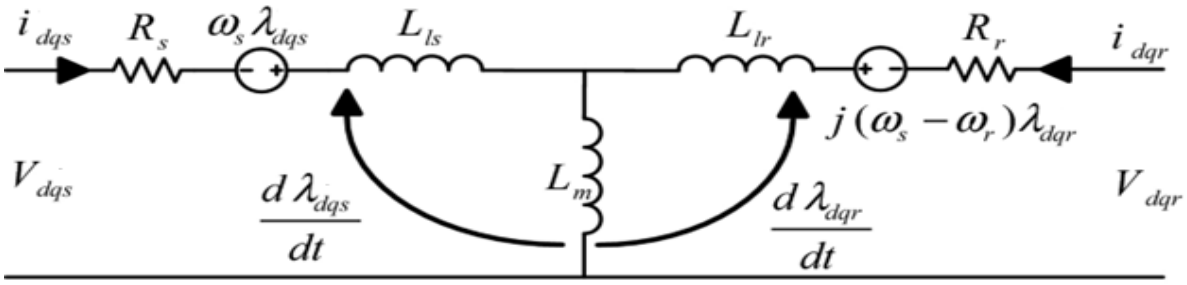

FIGURE 4. DFIG synchronous dq model.

B. DFIG MODELING

The DFIG is modeled in a synchronous q-d reference frame as illustrated in Fig.4 [28], [29].

The voltage (V_{ds}, V_{qs}) of stator winding can be written as follows:

$$V_{ds} = R_s i_{ds} - \omega_s \lambda_{qs} + \frac{d\lambda_{ds}}{dt} \tag{5}$$

$$V_{qs} = R_s i_{qs} + \omega_s \lambda_{ds} + \frac{d\lambda_{qs}}{dt} \tag{6}$$

The voltage (V_{dr}, V_{qr}) of rotor winding can be written as follows:

$$V_{dr} = R_r i_{dr} - s\omega_s \lambda_{qr} + \frac{d\lambda_{dr}}{dt} \tag{7}$$

$$V_{qr} = R_r i_{qr} + s\omega_s \lambda_{dr} + \frac{d\lambda_{qr}}{dt} \tag{8}$$

The linkage fluxes of both rotor (λ_{dr}, λ_{qr}) and stators (λ_{ds}, λ_{qs}) are described as follows:

$$\lambda_{ds} = L_{ls} i_{ds} + L_m i_{dr} \tag{9}$$

$$\lambda_{qs} = L i_{qs} + L_m i_{qr} \tag{10}$$

$$\lambda_{dr} = L i_{dr} + L_m i_{ds} \tag{11}$$

$$\lambda_{qr} = L_{lr} i_{qr} + L_m i_{qs} \tag{12}$$

where R_r and R_s are rotor and stator resistances respectively. L_{lr}, L_{ls}, and L_m are rotor self, stator self and mutual inductances, respectively. ω_s is defined as synchronous speed. i_{ds} and i_{qs} are dq stator currents. i_{dr} and i_{qr} are dq rotor currents.

C. ADAPTIVE FUZZY LOGIC CONTROLLER

Fuzzification, act rule base, and defuzzification are all part of the AFLC architecture. The block diagram of the provided AFLCs is shown in Fig.5. Following is an illustration of the AFLC PI design [21], [30]. The input of PI has been adjusted by the fuzzy logic regulator. Fig. 5 illustrates what is meant by the term ''adaptive control,'' which describes a fuzzy regulator whose features, such as the fuzzy rule, membership function, and output scaling factor, can vary in response to system change [31]. All factors (K_{Po}, K_{do}, K_o, K_P and K_i) have been adjusted for all six regulators to get the minimum integral square error (ISE). The Memberships are designated as positive big (PB), positive medium (PM), negative big (NB), positive small (PS), negative medium (NM), negative small (NS), and zero (Z), as shown in Fig. 6. One idea states that the input/output fuzzy sets are represented by the triangular membership functions (MFs) with overlap (PB) [32], [33]. The fuzzy inference employs 49 control rules to generate the proper signal, as illustrated in Table 1. Be aware

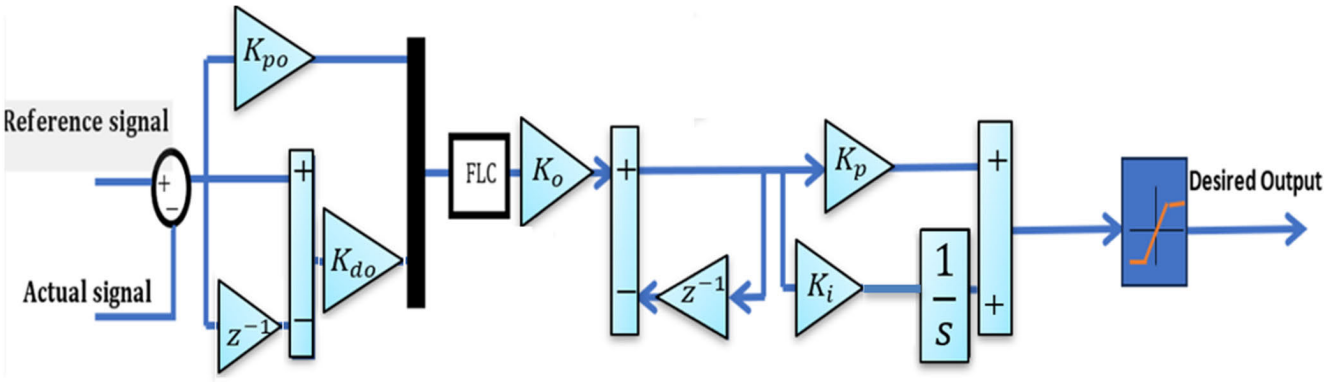

FIGURE 5. The AFLC scheme.

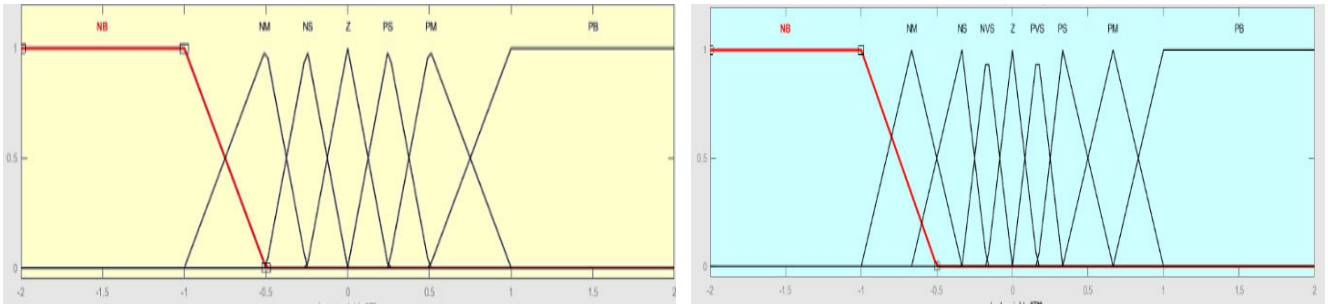

(a) (b)

FIGURE 6. Membership Functions; (a) for inputs; and (b) output.

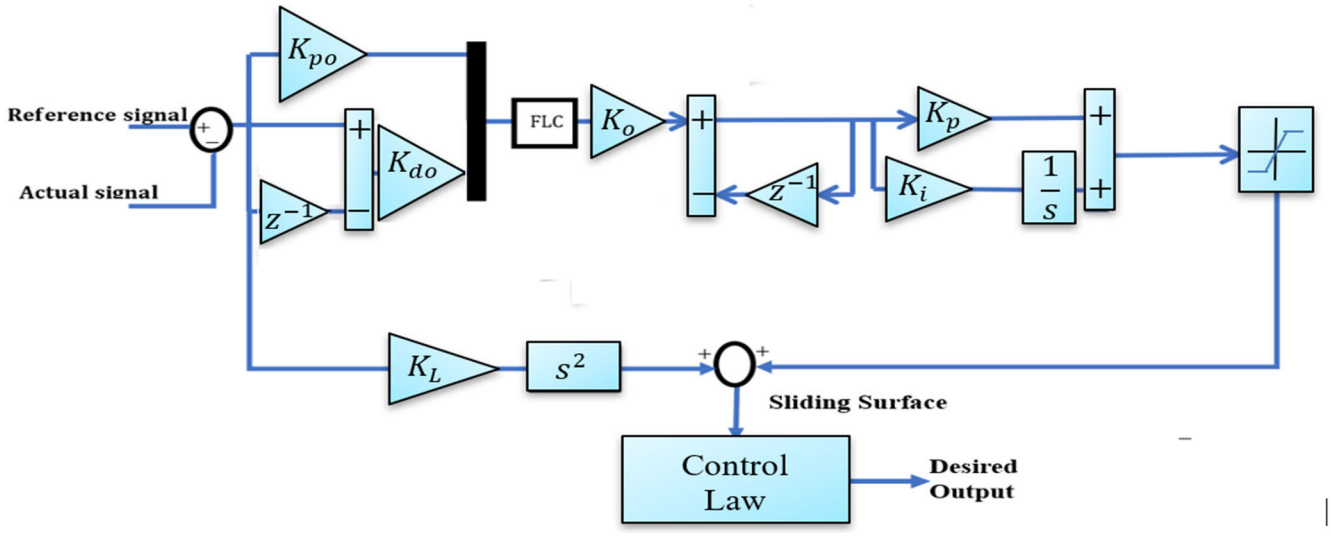

FIGURE 7. The SO-AFLC scheme.

that when the rules are created, the balance between projected inaccuracy and AFLC complexity is taken into consideration. The controller gains are optimized using Takagi-Sugeno optimization [34].

D. SECOND ORDER ADAPTIVE FUZZY LOGIC CONTROLLER

The main structure of the second-order adaptive fuzzy logic controller or second-order adaptive sliding mode controller

TABLE 1. AFLC rule base.

e / Δe	NB	NM	NS	Z	PS	PM	PB
NB	NB	NB	NB	NM	NS	NVS	Z
NM	NB	NB	NM	NS	NVS	Z	PVS
NS	NB	NM	NS	NVS	Z	PVS	PS
Z	NM	NS	NVS	Z	PVS	PS	PM
PS	NS	NVS	Z	PVS	PS	PM	PB
PM	NVS	Z	PVS	PS	PM	PB	PB
PB	Z	PVS	PS	PM	PB	PB	PB

(SO-ASMC) comprises two regulators, one of them is the adaptive fuzzy logic controller (AFLC) and the second one is the second-order sliding mode controller (SO-SMC). The positive benefits of both regulators are combined in SO-AFLC. The schematic diagram of the SO-AFLC is illustrated in Fig. 7. The AFLC is functioning in a state of steady activity and minimizes chatter in response. The SO-SMC is active during the system's transient state, providing a fast-dynamic response and improving the stability of the system. In the initial phase of SMC, the sliding surface (SS) is determined after the control rule is developed to guide the regulator to track the reference abruptly [35], [36], [37], [38], [39]. SS is determined using the error and its second derivative. The error and derivative of error are always directed towards SS in SMC. The controller gains are optimized using Takagi-Sugeno optimization [34]. SS is formulated as follows:

$$SS = K_L \ddot{e}(t) + \zeta(t) \tag{13}$$

where $\zeta(t)$ is the output of the AFLC.

Equation (14) is utilized in electrical systems where PWM is used to avoid oscillation and chattering issues.

$$Desired\ Output = -\Lambda \text{sat}(SS, \varrho) = -\Lambda \left[\frac{SS}{|SS| + \varrho}\right] \tag{14}$$

Λ is a tolerably large positive gain at $\varrho > 0$ and $\varrho \approx 0$.

E. ROTOR SIDE CONVERTER MODEL

RSC is used to control DFIG rotor speed so that it becomes possible to achieve maximum power point tracking from the random wind as shown in Fig. 8. The maximum power occurs at peak power coefficient which depends on pitch angle (β) and tip speed ratio (λ). Fig. 2 illustrates how to obtain the power coefficient's maximum value, which is 0.48. The λ should be locked at an optimal value which is 8.1 and the pitch angle must be at zero. So, in case of random wind speed, if the wind speed changes, the rotor speed of wind turbine will be adjusted in such a way as to cope with the change in the speed of the wind. To achieve this function, three controllers (1, 2, and 3) are used [6], [40].

F. GRID-SIDE CONVERTER MODEL

GSC is used to connect the generator to the utility grid as illustrated in Fig. 9. One of the major functions of GSC is to manage the power factor by controlling the reactive power and DC link voltage level. To achieve these functions three

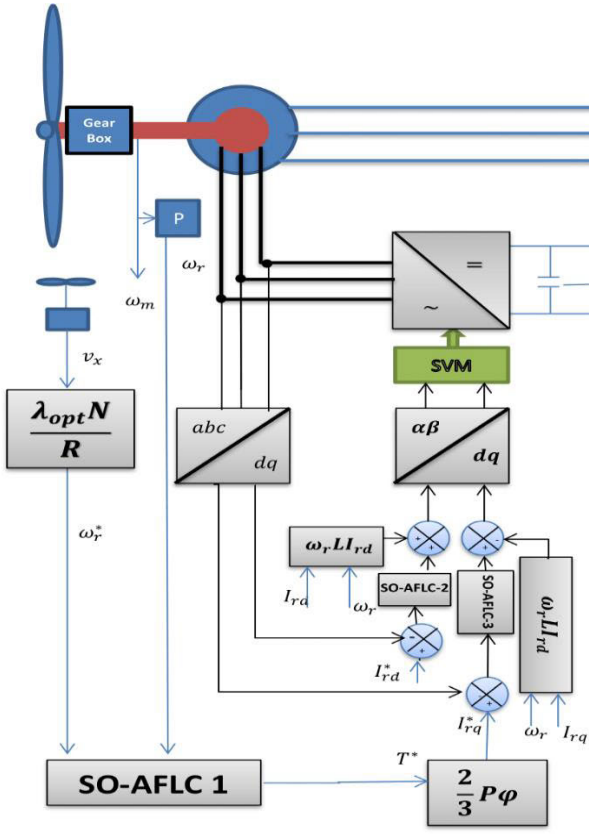

FIGURE 8. The RSC scheme.

controllers (4, 5, and 6) are used. It is very important to lock the DC link voltage at a constant value for the most efficient utilization of the power plant. Also, the unity power factor can be accomplished by locking the reactive power at zero [41], [42].

III. SIMULATION RESULTS

In this paper, the grid-tied DFIG wind power plant has been modeled using MATLAB/Simulink 2023a environment. The specification parameters for the system are illustrated in Table 2. The performance of SO-AFLC results has been investigated and discussed for both a step and a realistic wind speed profile. The purpose of this simulation is to validate the effectiveness of SO-AFLC in WPP and compare these results to the conventional PI controller and AFLC. The greatest gains for six controllers are described in Table 3. The PI gains (K_p and K_i) are optimized using the marine predator algorithm (MPA) [18].

A. CASE I: STEP WIND SPEED PROFILE

Case I discusses about the SO-AFLC results and contrasts them with AFLC and PI under a step wind speed profile. The speed profile is illustrated in Fig. 10. Fig. 11 shows the power coefficient (Cp) of the wind turbine under the three controllers. The power coefficient is adjusted at the optimum value (0.48). Both AFLC and SO-AFLC showed excellent

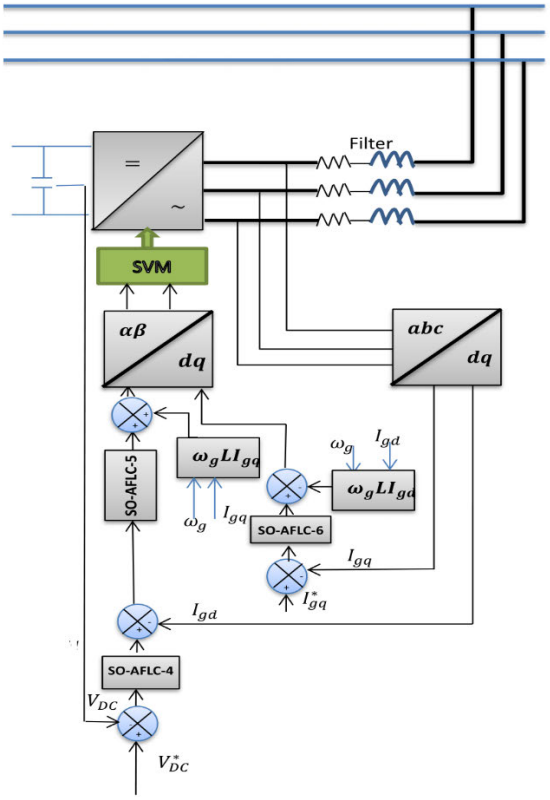

FIGURE 9. The GSC scheme.

TABLE 2. System parameters.

Parameter	Value
Nominal Power	$P_{nom} = 1650kw$
Voltage	$V_{nom} = 575V$
Frequency	$f = 50Hz$
Stator Resistance	$R_s = 0.0071pu$
Rotor Resistance	$R_r = 0.0050pu$
Stator Leakage inductance	$L_{ls} = 0.171pu$
Rotor Leakage inductance	$L_{lr} = 0.1560pu$
Magnetization inductance	$L_m = 2.9\ pu$
No. of Pair poles	$p = 3$

TABLE 3. Controllers parameters.

		Controller 1	Controller 2	Controller 3	Controller 4	Controller 5	Controller 6
PI	K_p	9.03	4.185	6.984	5.060	0.89	3.287
	K_i	4.283	1.581	3.91	1.628	2.013	1.256
AFLC	K_0	0.1563	2.258	0.312	0.9815	1.246	2.4902
	K_{po}	10.759	5.236	1.688	8.146	0.177	8.012
	K_{do}	4.589	1.549	2.516	0.2789	5.8721	0.0154
	K_p	9.756	5.214	8.345	1.6345	0.0023	6.567
	K_i	4.659	1.248	0.2789	0.544	6.234	0.002
SO-AFLC	K_0	2.538	3.689	0.254	1.003	1.756	3.523
	K_{po}	14.189	5.869	1.007	8.023	0.225	8.443
	K_{do}	6.698	1.869	3.681	0.3892	7.78	0.254
	K_p	10.268	7.456	9.355	1.7455	0.35	8.546
	K_i	5.272	2.528	2.6029	0.714	9.005	0.0001
	K_L	3.3	1.8	1.9	1.6	1.14	2.002

promising results compared to PI with slight improvement for the SO-AFLC. At t = 1 s and t = 3 s, SO-AFLC has a

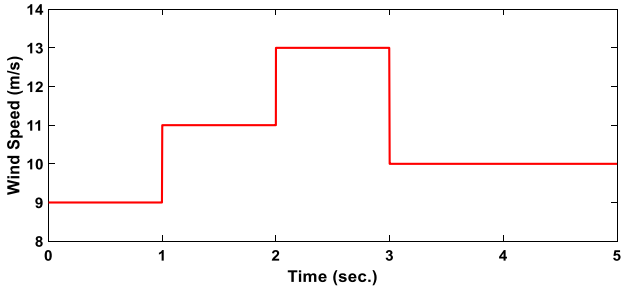

FIGURE 10. Wind speed profile.

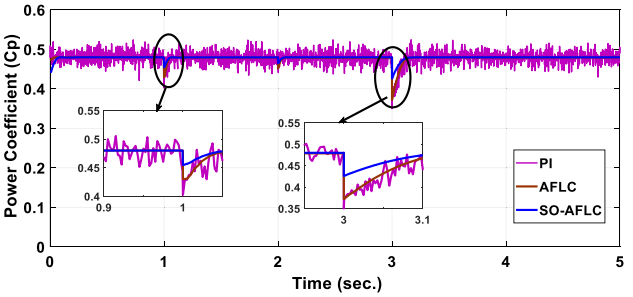

FIGURE 11. Power coefficient.

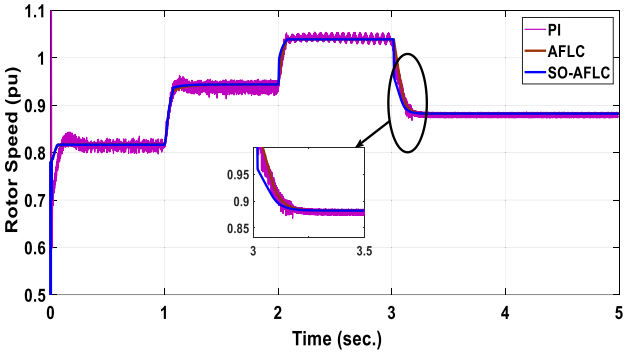

FIGURE 12. The rotor speed of DFIG.

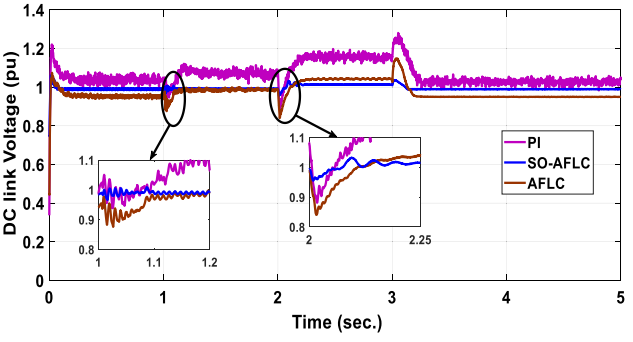

FIGURE 13. DC link Voltage between RSC and GSC.

lower undershoot compared to AFLC. In comparison to the PI controller and AFLC, SO-AFLC has reduced the steady-state error in the Cp waveform by 63.25% and 13.12%, respectively. Fig. 12 describes the rotational speed of the rotor of DFIG. Both SO-AFLC and AFLC have better speed tracking

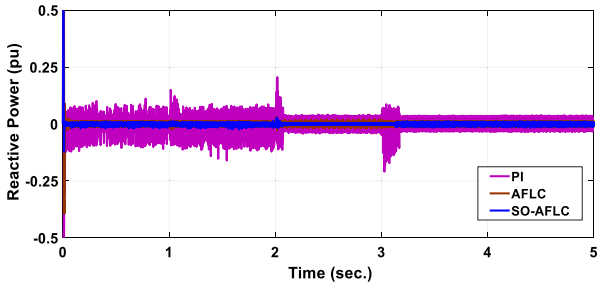

FIGURE 14. Grid injected reactive power.

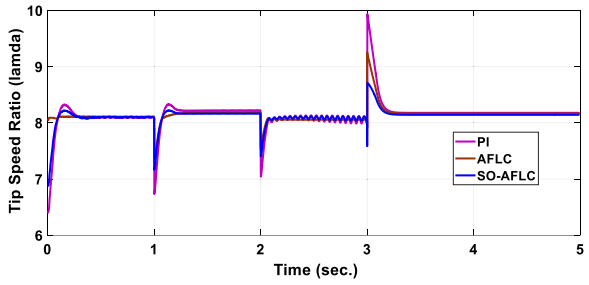

FIGURE 15. TIP speed ratio.

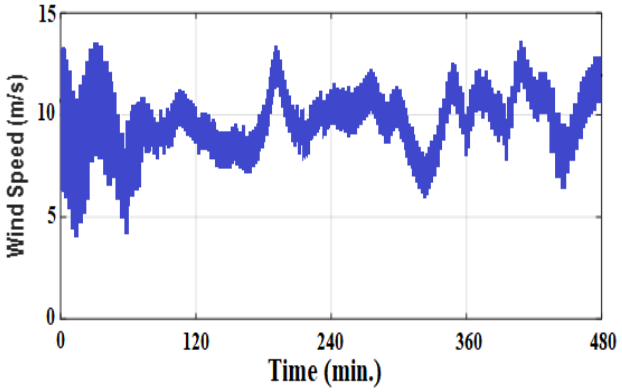

FIGURE 16. Realistic wind speed data.

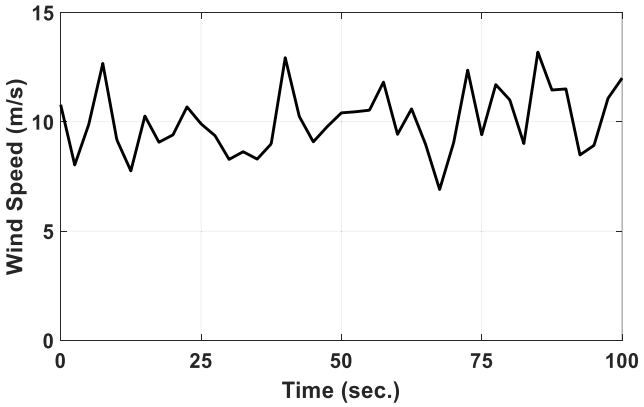

FIGURE 17. Wind speed profile.

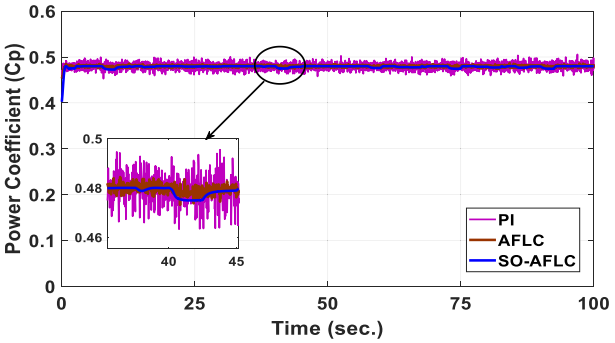

FIGURE 18. Power coefficient.

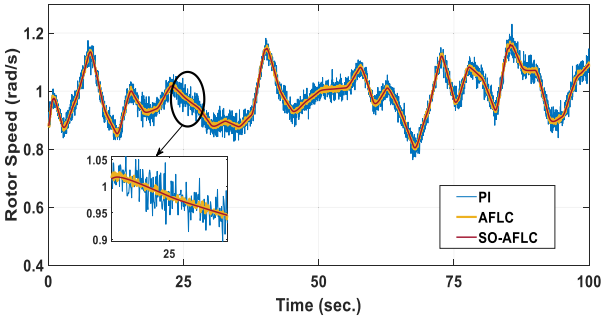

FIGURE 19. The rotor speed of DFIG.

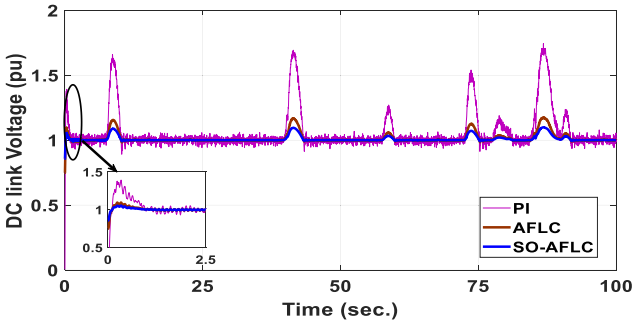

FIGURE 20. DC link Voltage between RSC and GSC.

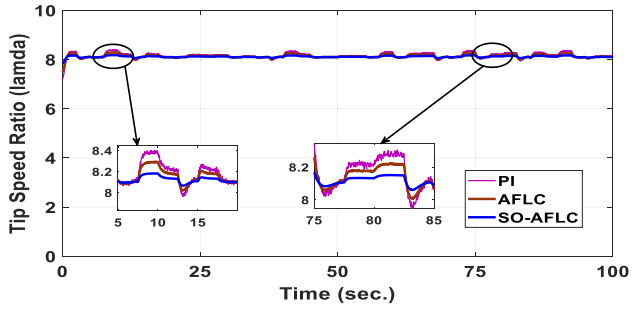

FIGURE 21. Tip speed ratio.

than PI with slight enhancement for SO-AFLC. At t = 3 s, SO-AFLC showed a quicker response than AFLC and PI. The SO-AFLC improved the rotational speed tracking by 76.32% compared to PI and 16.1% compared to AFLC. The DC link voltage between RSC and GSC is illustrated in Fig. 13. Between t = 2 s and t =3 s, SO-AFLC and AFLC

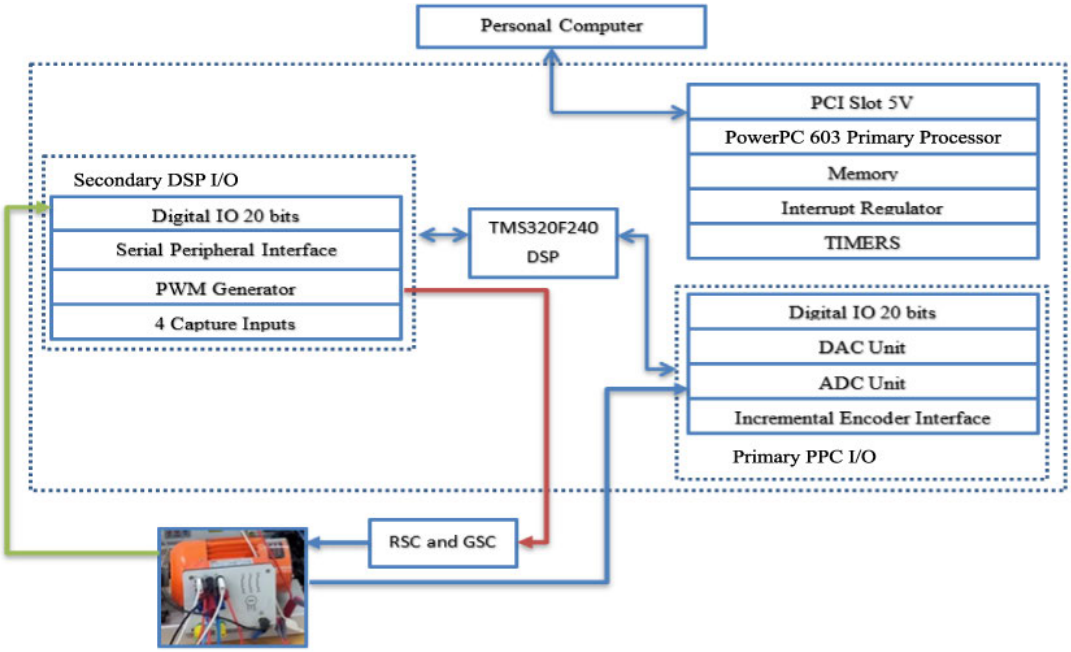

FIGURE 22. DSP 1104 controller card block diagram.

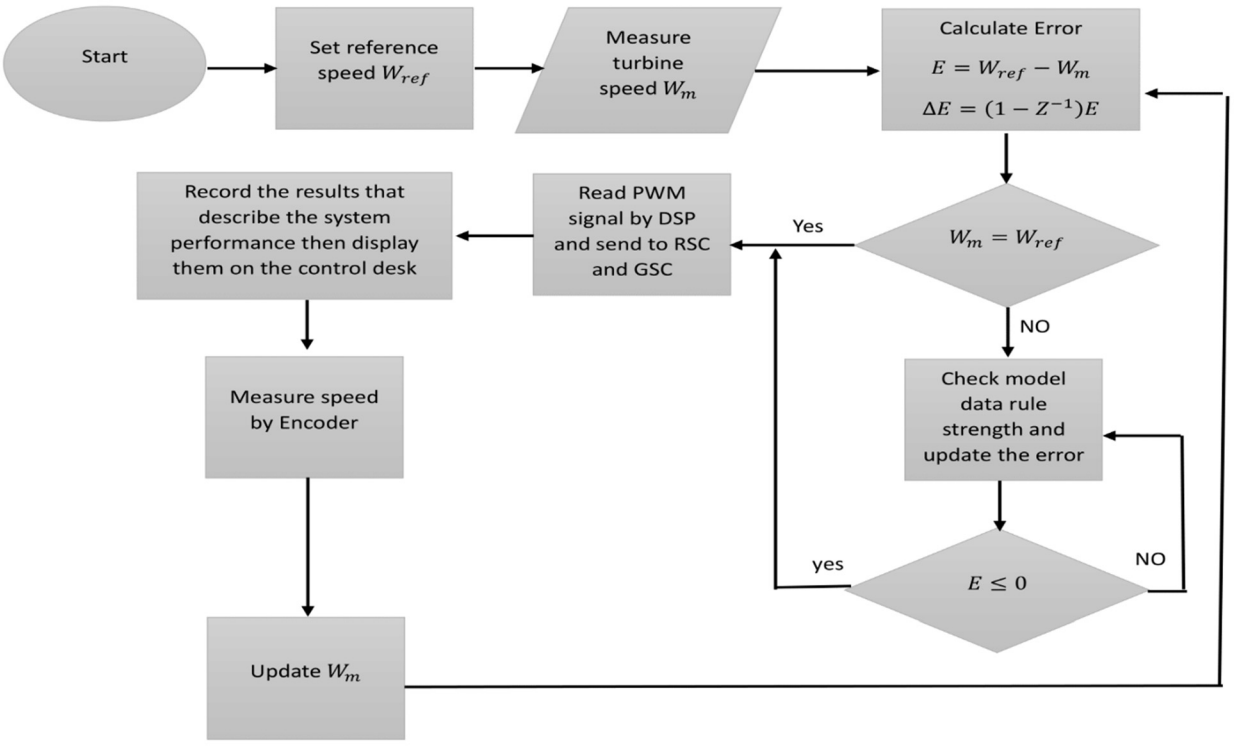

FIGURE 23. The experimental Laboratory flowchart.

have the lowest steady-state error for DC link voltage at high wind speed. At t =1 s and t = 2 s, SO-AFLC has the lowest undershooting compared to AFLC and PI. At t = 3 s, SO-AFLC has the lowest peak overshoot. In Fig. 14, the reactive power value is adjusted at zero to keep the unity power factor. Both SO-AFLC and AFLC have the

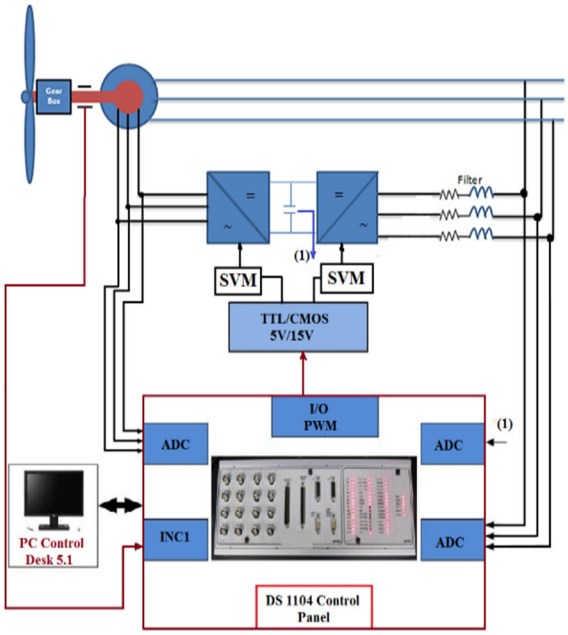

FIGURE 24. Schematic laboratory setup.

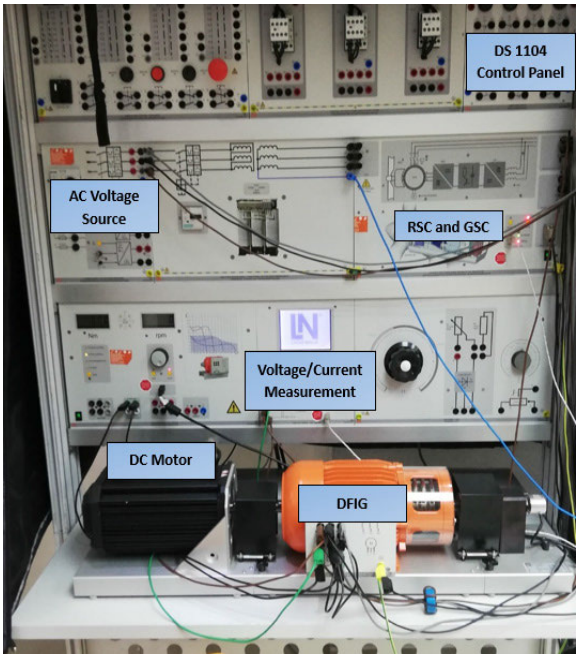

FIGURE 25. The experimental hardware.

lowest error and the best reactive power tracking compared to PI. SO-AFLC has slightly fewer errors than AFLC. In Fig. 15, the tip speed ratio is adjusted at the optimum value of 8.1 for the three controllers. At t = 3 s, SO-AFLC has reduced peak overshoot compared to PI and AFLC. Between t = 2 s and t = 3 s, both SO-AFLC and AFLC have the lowest steady-state error with slight improvement for SO-AFLC.

TABLE 4. Analysis of the IAE values.

	PI	AFLC	SO-AFLC
Controller -1	0.064	0.023	0.013
Controller -2	0.059	0.003	0.002
Controller -3	0.153	0.112	0.087
Controller -4	0.326	0.126	0.098
Controller -5	0.0213	0.0128	0.0067
Controller -6	0.0126	0.00828	0.0053
Mean square	0.02298	0.004865	0.0029

B. CASE II: REAISTIC WIND SPEED PROFILE

Case II discusses the results of SO-AFLC and compares them to AFLC and PI under a realistic wind profile from Ras Gareb at the Gulf of Suez in Egypt. The average monthly speed of the wind at Ras Gareb changes from 15 m/s (August) to 7.5 m/s (January) [43]. The realistic wind speed measured from Ras Gareb is illustrated in Fig. 16. The data is measured for 480 mins. The data is scaled and reprocessed for 100 seconds to fit both experimental and simulation specifications. Fig. 17 illustrates the symbolized profile of the wind speed from Ras Gareb. The power coefficient Cp of the wind turbine under the three controllers is illustrated in Fig. 18. The power coefficient is adjusted at the optimum value (0.48). Both AFLC and SO-AFLC showed great results compared to PI with advance for the SO-AFLC. Between t = 40 s and t = 45 s, SO-AFLC has a lower undershoot compared to AFLC and PI. SO-AFLC has improved the steady-state error in the Cp waveform by 62.32% compared to the PI controller and 10.26% compared to AFLC. Fig. 19 describes the rotational speed of the rotor of DFIG. Both SO-AFLC and AFLC have better speed tracking than PI. SO-AFLC showed a faster response than AFLC and PI. The SO-AFLC improved the rotational speed tracking by 72.51% compared to PI and 12.23% compared to AFLC. The DC link voltage between RSC and GSC is illustrated in Fig. 20. GSC is used to regulate the DC link voltage at a fixed value. At high wind speeds, SO-AFLC and AFLC have the lowest overshoot for DC link voltage with slight improvement for SO-AFLC. SO-AFLC has the lowest steady-state error compared to AFLC and PI. In Fig. 21, the tip speed ratio is adjusted at the optimum value of 8.1 for the three controllers. SO-AFLC has reduced steady-state error compared to PI and AFLC. Between t = 5 s and t = 15 s, both SO-AFLC and AFLC have the lowest peak overshoot with slight improvement for SO-AFLC.

The suggested SO-AFLCs have improved behaviors that enable maximum power tracking and the restoration of system responses to their steady-state performance. In addition, a comparison of tracking errors may be made using the integral absolute error (IAE) as shown below for the best evaluation of the system:

$$IAE = \int_0^\infty |e(t)|\, dt \tag{15}$$

The tracking errors of the PI, AFLC and SO-AFLC using all six controllers are based on Table 4. The mean square error is

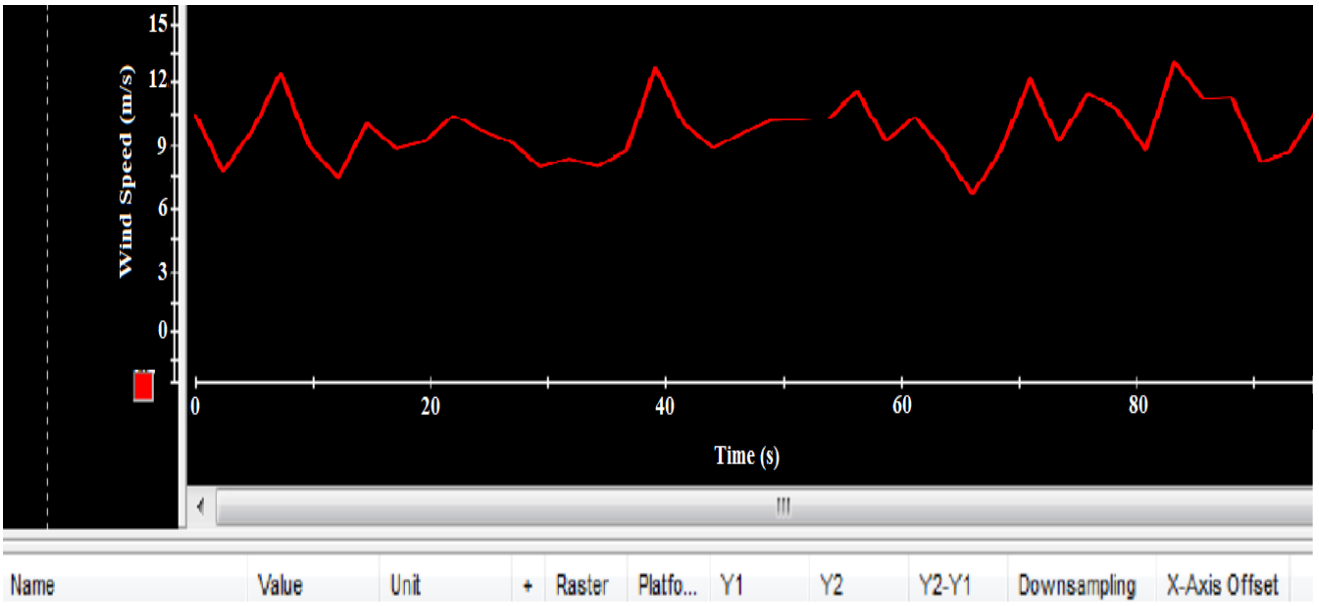

FIGURE 26. Experimental wind speed profile.

reduced by 87.38% compared to PI and by 40.39% compared to AFLC.

IV. DS 1104 CONTROL BOARD

The Controller Card (DS 1104) is a low-cost featuring a real-time processor that can be installed on a personal computer with a free PCI 5 V slot. It can be used with Simulink/Matlab software to develop and test control systems. The Dspace system integrates well with Simulink/Matlab, providing a powerful and efficient environment. The Real-Time Interface can easily transfer function models to the dSPACE system. The ControlDesk software 4.2 can be used to set up the input and output of the control system graphically. The Simulink Coder generates code for the model, which is compiled, downloaded, and started automatically on the Dspace system. This seamless integration between Dspace and Simulink/Matlab decreases time and cost and increases productivity. The DS1104 Card block diagram is illustrated in Fig. 22. It consists of a main processor (Power PC 64-bit processor with 250 MHz CPU), a secondary DSP I/O subsystem, and a primary PPC I/O subsystem. The dSPACE controller card also includes a software package for operating the card through the Simulink. The experiment consists of two aspects. The hardware aspect is a control board that allows generating PWM control signals. The software aspect is the DSP-to-MATLAB interface libraries on Matlab/Simulink. SO-AFLC has been simulated on Matlab using fuzzy toolbox, DSP-to-MATLAB interface libraries, and real-time interface to Simulink which are placed on the personal computer [44], [45]. Figure 23 illustrates the experimental laboratory flowchart arrangement.

V. EXPERIMENTAL RESULTS

A laboratory hardware of the system was constructed using the DS 1104 control board to validate the simulation outcomes and validate the viability of the proposed controller. Fig.24 illustrates the connection between the experimental setup based on DSP 1104 control board. Fig.25 shows the real hardware test for the laboratory setup. The system consists of DFIG (4-poles, 270 W, 230/400 V, pf 1/0.75, 3.2/2 Amp, 50 Hz), Prime mover (250W, with separately excited DC motor, 180/220VDC, 3000 rpm), Position and speed sensor (incremental encoder Speed: 6000 rpm, 1024 pulses, Moment of inertia: 35 gcm^2), current and measurement device and DC chopper control circuit (IGBT 600V, $50A_{SC}$, IR2110, $500V_{offset}$, super-fast rectifiers MUR 2060, Diode 1n5819). The DC motor is used to represent wind speed. A DFIG is directly linked to a DC motor, which serves as the prime mover. Utilizing an incremental encoder, a digital signal representing the actual speed of the rotor is generated and delivered to DS 1104.

The speed profile illustrated in Fig. 26 represents a realistic wind profile from Ras Gareb in the Gulf of Suez, Egypt. Fig. 27 describes the rotational speed of the rotor of DFIG. Both SO-AFLC and AFLC have better speed tracking than PI. SO-AFLC shown in Fig. 27 (c) provides a faster response than AFLC (Fig. 27 (b)) and PI (Fig.27 (a)). The experimental validation has shown that SO-AFLC improved the rotational speed tracking with lower error compared to PI and AFLC.

The wind turbine's power coefficient (Cp) under the three controllers is depicted in Fig. 28. It is adjusted to the optimum value of 0.48. In comparison to PI, both AFLC and SO-AFLC demonstrated excellent results with slight advances for the

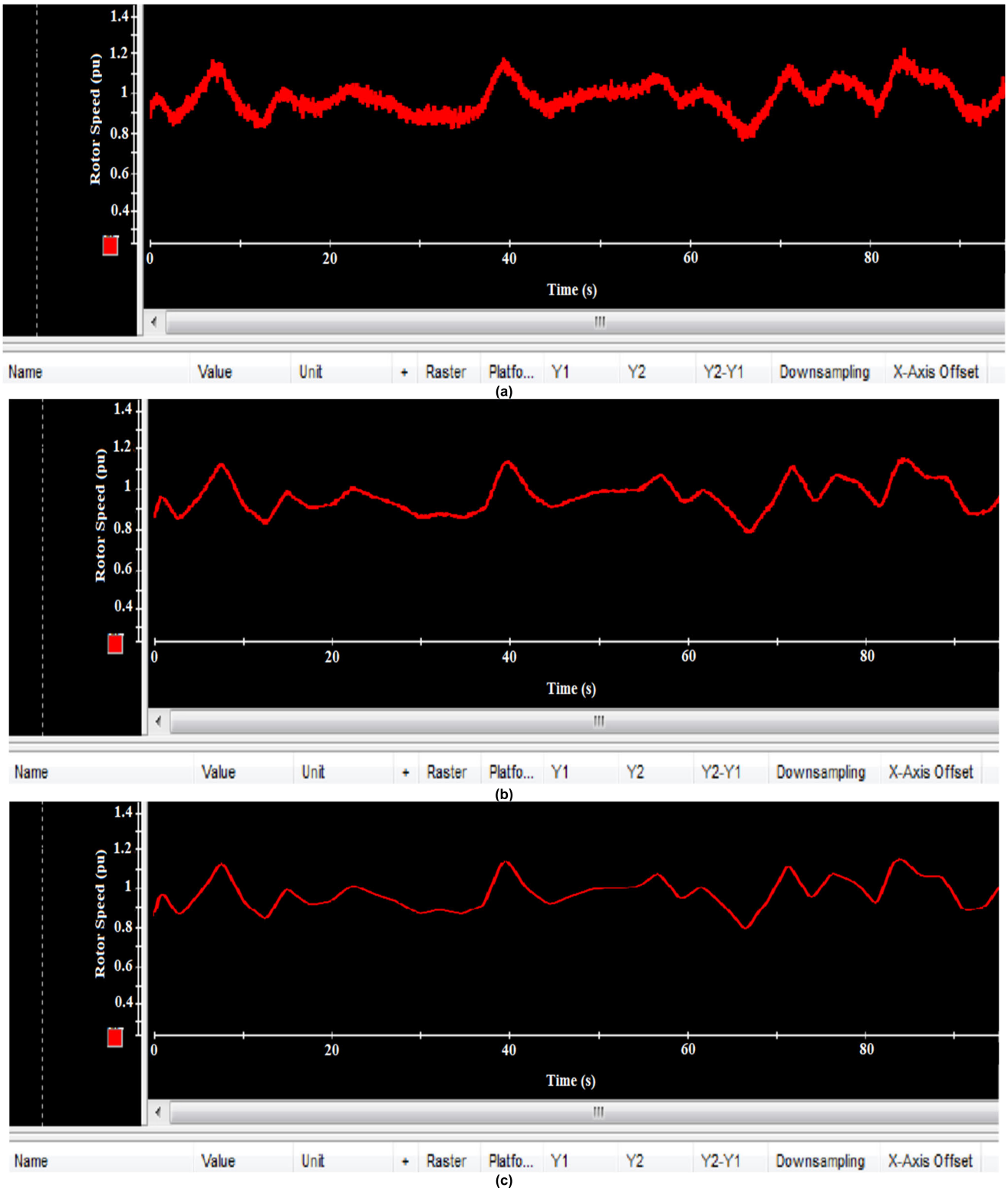

FIGURE 27. Experimental rotational speed results using (a) PI, (b) AFLC, and (c) SO-AFLC.

SO-AFLC. In comparison to AFLC and PI, SO-AFLC had less undershoot between t = 40 s and t = 45 s. Comparing SO-AFLC to PI controller and AFLC, the steady-state error in the Cp waveform has improved.

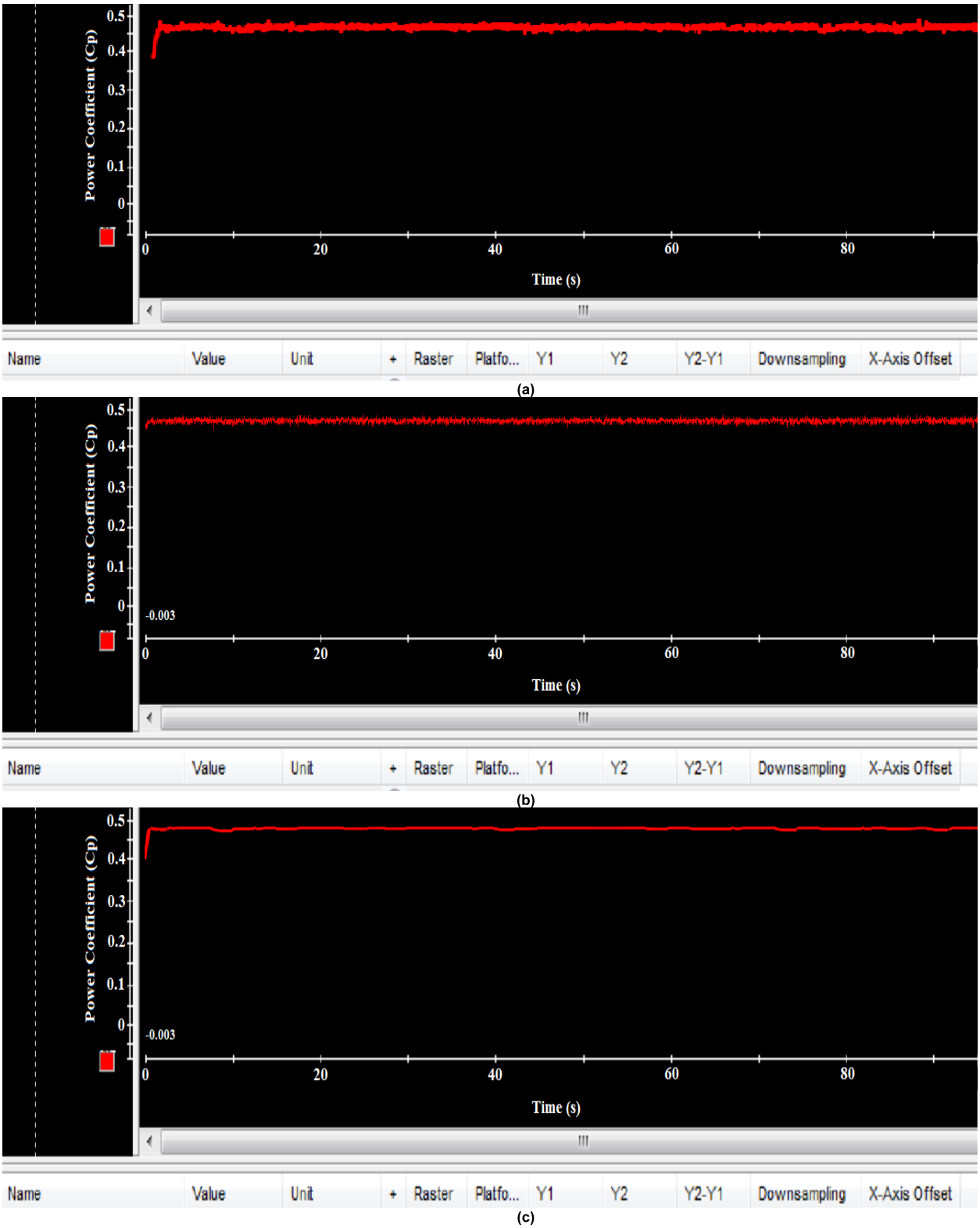

FIGURE 28. Experimental power coefficient results using (a) PI, (b) AFLC, and (c) SO-AFLC.

In Fig. 29, the tip speed ratio is set to its optimum value of 8.1 for the three controllers. Comparing SO-AFLC to the PI and AFLC, steady-state error has been minimized. Both SO-AFLC and AFLC exhibit the lowest peak overshoot between t = 5 s and t = 15 s, with SO-AFLC showing a slight improvement.

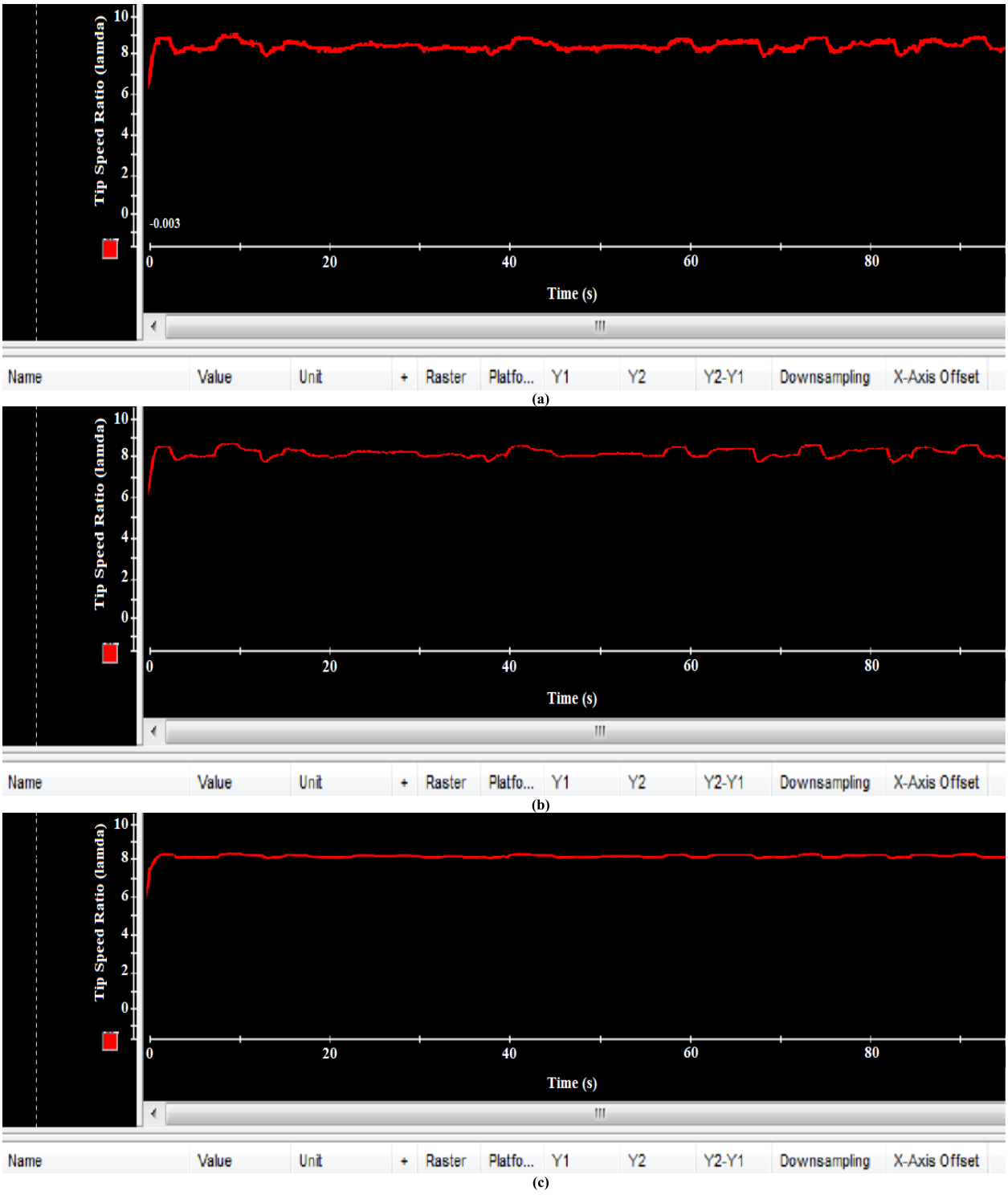

FIGURE 29. Experimental tip speed ratio results using (a) PI, (b) AFLC, and (c) SO-AFLC.

The DC link voltage between GSC and RSC is illustrated in Fig. 30. GSC is used to control the DC link voltage at a constant value. At high wind speeds, SO-AFLC and AFLC have the lowest overshoot for DC link voltage with slight improvement for SO-AFLC. SO-AFLC has the lowest steady-state error compared to AFLC and PI.

The experimental results are very acceptable when they are compared to simulation results. The findings have proven when SO-AFLC is used as an option instead of PI and AFLC,

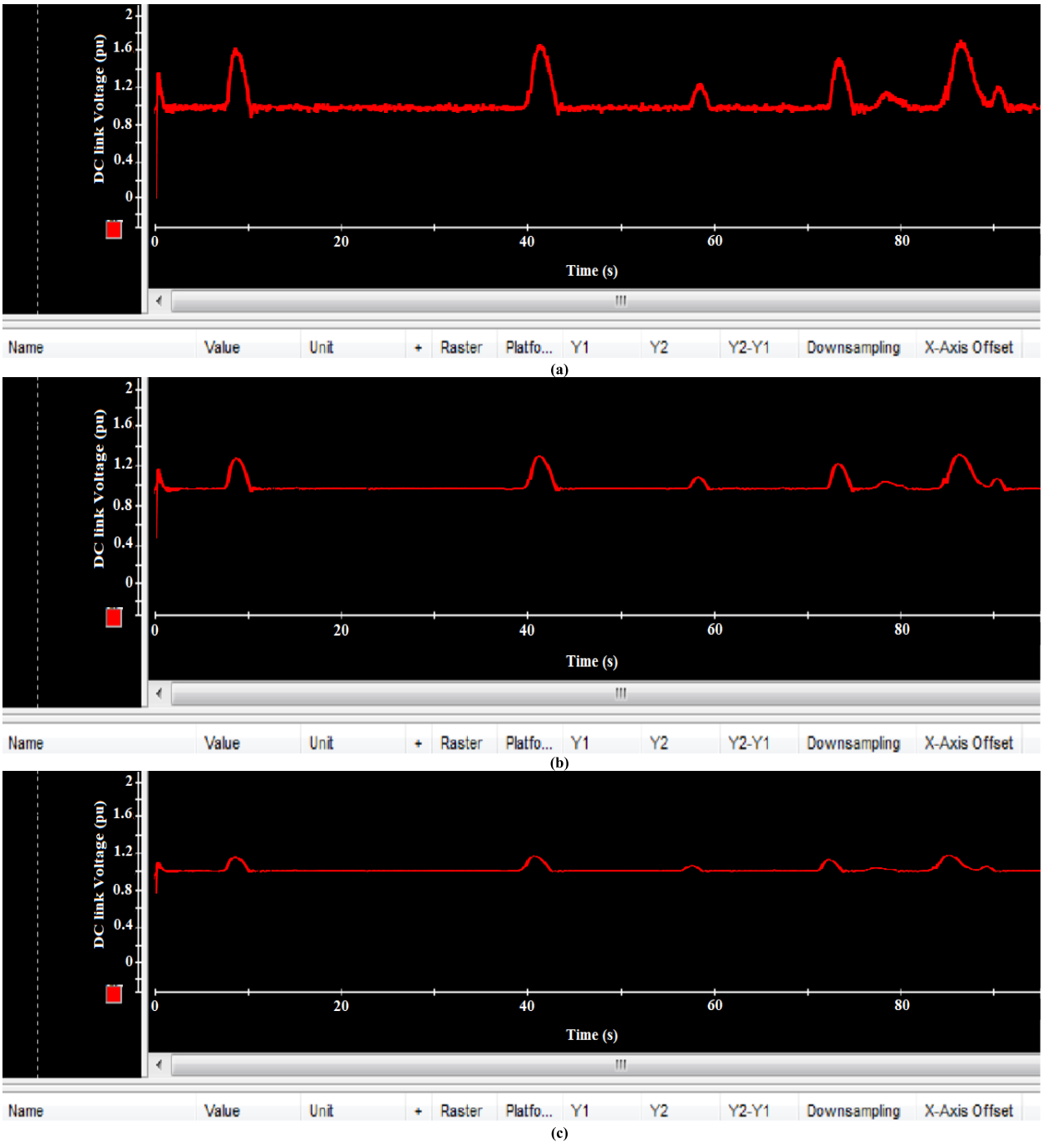

FIGURE 30. Experimental DC link voltage results using (a) PI, (b) AFLC, and (c) SO-AFLC.

the grid-tied DFIG WPP performance shows better maximum power tracking, speed tracking, and very good DC link voltage tracking.

VI. CONCLUSION

This article validates the effectiveness of SO-AFLC for grid-tied DFIG. The SO-AFLC technique for DFIG-based wind generation systems was discussed in terms of simulation and real-time implementation. The DSpace DS1104 control board is used for experimental verification. The experimental test confirms the simulation model's success by comparing the findings under identical run-time and wind-speed profile conditions. In comparison to PI and AFLC, the employing of SO-AFLCs gave results with a quick time response, a high rate of convergence, less peak overshoot, less undershoot, and minimum steady-state error. Under the unit step wind speed profile, SO-AFLC has improved the steady-state error in the Cp waveform by 63.25% compared to the PI controller and

13.12% compared to AFLC. Under the wind profile obtained from Ras Gareb, SO-AFLC has lower undershoot compared to AFLC and PI. SO-AFLC has improved the steady-state error in the Cp waveform by 62.32% compared to the PI controller and 10.26% compared to AFLC. The SO-AFLC improved the rotational speed tracking by 72.51% compared to the PI and 12.23% compared to AFLC.

REFERENCES

[1] D. Song, Y. Yang, S. Zheng, X. Deng, J. Yang, M. Su, W. Tang, X. Yang, L. Huang, and Y. H. Joo, "New perspectives on maximum wind energy extraction of variable-speed wind turbines using previewed wind speeds," *Energy Convers. Manage.*, vol. 206, Feb. 2020, Art. no. 112496.

[2] D. Song, J. Liu, J. Yang, M. Su, S. Yang, X. Yang, and Y. H. Joo, "Multi-objective energy-cost design optimization for the variable-speed wind turbine at high-altitude sites," *Energy Convers. Manage.*, vol. 196, pp. 513–524, Sep. 2019.

[3] M. Yesilbudak, "Implementation of novel hybrid approaches for power curve modeling of wind turbines," *Energy Convers. Manage.*, vol. 171, pp. 156–169, Sep. 2018.

[4] L. Yang, Z. Xu, J. Ostergaard, Z. Y. Dong, and K. P. Wong, "Advanced control strategy of DFIG wind turbines for power system fault ride through," *IEEE Trans. Power Syst.*, vol. 27, no. 2, pp. 713–722, May 2012.

[5] M. Yin, Y. Xu, C. Shen, J. Liu, Z. Y. Dong, and Y. Zou, "Turbine stability-constrained available wind power of variable speed wind turbines for active power control," *IEEE Trans. Power Syst.*, vol. 32, no. 3, pp. 2487–2488, May 2017.

[6] W. S. E. Abdellatif, A. M. Hamada, and S. A. M. Abdelwahab, "Wind speed estimation MPPT technique of DFIG-based wind turbines theoretical and experimental investigation," *Electr. Eng.*, vol. 103, no. 6, pp. 2769–2781, Dec. 2021.

[7] Y. A. Eldahab, N. H. Saad, and A. Zekry, "Assessing wind energy conversion systems based on newly developed wind turbine emulator," *Int. J. Smart Grid*, vol. 4, no. 4, pp. 140–148, Dec. 2020.

[8] R.-E. Precup, T. Kamal, and S. Z. Hassan, "Sensitivity analysis of frequency regulation parameters in power systems with wind generation," in *Advanced Control and Optimization Paradigms for Wind Energy Systems*. Singapore: Springer, 2019, pp. 67–88.

[9] K. Ni, Y. Hu, D. T. Lagos, G. Chen, Z. Wang, and X. Li, "Highly reliable back-to-back power converter without redundant bridge arm for doubly fed induction generator-based wind turbine," *IEEE Trans. Ind. Appl.*, vol. 55, no. 3, pp. 3024–3036, May 2019.

[10] A. W. H. Lio and F. Meng, "Effective wind speed estimation for wind turbines in down-regulation," *J. Phys., Conf. Ser.*, vol. 1452, no. 1, Jan. 2020, Art. no. 012008.

[11] M. Yessef, B. Bossoufi, M. Taoussi, S. Motahhir, A. Lagrioui, H. Chojaa, S. Lee, B.-G. Kang, and M. Abouhawwash, "Improving the maximum power extraction from wind turbines using a second-generation CRONE controller," *Energies*, vol. 15, no. 10, p. 3644, May 2022.

[12] S. Musunuri and H. L. Ginn, "Comprehensive review of wind energy maximum power extraction algorithms," in *Proc. IEEE Power Energy Soc. Gen. Meeting*, Jul. 2011, pp. 1–8.

[13] M. A. Abdullah, A. H. M. Yatim, C. W. Tan, and R. Saidur, "A review of maximum power point tracking algorithms for wind energy systems," *Renew. Sustain. Energy Rev.*, vol. 16, no. 5, pp. 3220–3227, Jun. 2012.

[14] A. A. Salem, N. A. N. Aldin, A. M. Azmy, and W. S. E. Abdellatif, "Implementation and validation of an adaptive fuzzy logic controller for MPPT of PMSG-based wind turbines," *IEEE Access*, vol. 9, pp. 165690–165707, 2021.

[15] M. Cheng and Y. Zhu, "The state of the art of wind energy conversion systems and technologies: A review," *Energy Convers. Manage.*, vol. 88, pp. 332–347, Dec. 2014.

[16] Y. Mousavi, G. Bevan, I. B. Küçükdemiral, and A. Fekih, "Maximum power extraction from wind turbines using a fault-tolerant fractional-order nonsingular terminal sliding mode controller," *Energies*, vol. 14, no. 18, p. 5887, Sep. 2021.

[17] Y. Ihedrane, C. E. Bekkali, B. Bossoufi, and M. Bouderbala, "Control of power of a DFIG generator with MPPT technique for wind turbines variable speed," *Model., Identificat. Control Methods Renew. Energy Syst.*, vol. 1, pp. 105–129, Dec. 2018.

[18] R. G. Mohamed, M. A. Ebrahim, Z. M. Alaas, and M. M. R. Ahmed, "Optimal energy harvesting of large-scale wind farm using marine predators algorithm," *IEEE Access*, vol. 10, pp. 24995–25004, 2022.

[19] Z. Mekrini and S. Bri, "Performance of an indirect field-oriented control for asynchronous machine," *Int. J. Eng. Technol.*, vol. 8, no. 2, pp. 726–733, 2016.

[20] E. Bekiroglu and M. D. Yazar, "MPPT control of grid connected DFIG at variable wind speed," *Energies*, vol. 15, no. 9, p. 3146, Apr. 2022.

[21] M. M. Gulzar, D. Sibtain, A. F. Murtaza, S. Murawwat, M. Saadi, and A. Jameel, "Adaptive fuzzy based optimized proportional-integral controller to mitigate the frequency oscillation of multi-area photovoltaic thermal system," *Int. Trans. Electr. Energy Syst.*, vol. 31, no. 1, Jan. 2021, Art. no. e12643.

[22] K. Zeb, Z. Ali, K. Saleem, W. Uddin, M. A. Javed, and N. Christofides, "Indirect field-oriented control of induction motor drive based on adaptive fuzzy logic controller," *Electr. Eng.*, vol. 99, no. 3, pp. 803–815, Sep. 2017.

[23] K. D. Eddine, A. Mezouar, L. Boumediene, and A. P. M. van den Bossche, "A comprehensive review of LVRT capability and sliding mode control of grid-connected wind-turbine-driven doubly fed induction generator," *Automatika, Èasopis za Automatiku, Mjerenje*, vol. 57, no. 4, pp. 922–935, Oct. 2016.

[24] Y. Liu, Z. Wang, L. Xiong, J. Wang, X. Jiang, G. Bai, R. Li, and S. Liu, "DFIG wind turbine sliding mode control with exponential reaching law under variable wind speed," *Int. J. Electr. Power Energy Syst.*, vol. 96, pp. 253–260, Mar. 2018.

[25] R. F. Nayeh, H. Moradi, and G. Vossoughi, "Multivariable robust control of a horizontal wind turbine under various operating modes and uncertainties: A comparison on sliding mode and H_∞ control," *Int. J. Electr. Power Energy Syst.*, vol. 115, Feb. 2020, Art. no. 105474.

[26] B. Meghni, D. Dib, and A. T. Azar, "A second-order sliding mode and fuzzy logic control to optimal energy management in wind turbine with battery storage," *Neural Comput. Appl.*, vol. 28, no. 6, pp. 1417–1434, Jun. 2017.

[27] A. Tadesse, E. Ayenew, and L. Venkata, "Direct adaptive fuzzy PI strategy for a smooth MPPT of variable speed wind turbines," in *Proc. 8th EAI Int. Conf. Adv. Sci. Technol. (ICAST)*. Bahir Dar, Ethiopia: Springer, 2021, pp. 351–360.

[28] A. Ghasemi, M. H. Refan, and P. Amiri, "Enhancing the performance of grid synchronization in DFIG-based wind turbine under unbalanced grid conditions," *Electr. Eng.*, vol. 102, no. 3, pp. 1175–1194, Sep. 2020.

[29] M. K. Döşoğlu, "Nonlinear dynamic modeling for fault ride-through capability of DFIG-based wind farm," *Nonlinear Dyn.*, vol. 89, no. 4, pp. 2683–2694, Sep. 2017.

[30] K. Zeb, S. U. Islam, W. U. Din, I. Khan, M. Ishfaq, T. D. C. Busarello, I. Ahmad, and H. J. Kim, "Design of fuzzy-PI and fuzzy-sliding mode controllers for single-phase two-stages grid-connected transformerless photovoltaic inverter," *Electronics*, vol. 8, no. 5, p. 520, May 2019.

[31] O. Zamzoum, A. Derouich, S. Motahhir, Y. El Mourabit, and A. El Ghzizal, "Performance analysis of a robust adaptive fuzzy logic controller for wind turbine power limitation," *J. Cleaner Prod.*, vol. 265, Aug. 2020, Art. no. 121659.

[32] B. E. Elnaghi, M. N. Abelwhab, A. M. Ismaiel, and R. H. Mohammed, "Solar hydrogen variable speed control of induction motor based on chaotic billiards optimization technique," *Energies*, vol. 16, no. 3, p. 1110, Jan. 2023.

[33] R. H. Mohammed, A. M. Ismaiel, B. E. Elnaghi, and M. E. Dessouki, "African vulture optimizer algorithm based vector control induction motor drive system," *Int. J. Electr. Comput. Eng. (IJECE)*, vol. 13, no. 3, p. 2396, Jun. 2023.

[34] R. Ratrey and M. S. R. Dewangan, "A review on wind power generation using neural and fuzzy logic," *Int. Res. J. Eng. Technol.*, vol. 8, no. 4, pp. 4187–4193, Apr. 2021.

[35] A. Saghafinia, H. W. Ping, M. N. Uddin, and K. S. Gaeid, "Adaptive fuzzy sliding-mode control into chattering-free IM drive," *IEEE Trans. Ind. Appl.*, vol. 51, no. 1, pp. 692–701, Jan. 2015.

[36] F. F. M. El-Sousy, "Adaptive dynamic sliding-mode control system using recurrent RBFN for high-performance induction motor servo drive," *IEEE Trans. Ind. Informat.*, vol. 9, no. 4, pp. 1922–1936, Nov. 2013.

[37] S. Kochetkov, S. A. Krasnova, and V. A. Utkin, "The new second-order sliding mode control algorithm," *Mathematics*, vol. 10, no. 13, p. 2214, Jun. 2022.

[38] J. Chen, Z. Shuai, H. Zhang, and W. Zhao, "Path following control of autonomous four-wheel-independent-drive electric vehicles via second-order sliding mode and nonlinear disturbance observer techniques," *IEEE Trans. Ind. Electron.*, vol. 68, no. 3, pp. 2460–2469, Mar. 2021.
[39] S. Ding, J. H. Park, and C.-C. Chen, "Second-order sliding mode controller design with output constraint," *Automatica*, vol. 112, Feb. 2020, Art. no. 108704.
[40] G. B. A. Kumar and Shivashankar, "Optimal power point tracking of solar and wind energy in a hybrid wind solar energy system," *Int. J. Energy Environ. Eng.*, vol. 13, no. 1, pp. 77–103, Mar. 2022.
[41] K. R. Gogulamoodi, S. M. Shaby, and P. Ramesh, "Maximum power point tracking algorithm for grid-connected photo voltaic system," *J. Phys., Conf. Ser.*, vol. 1172, Mar. 2019, Art. no. 012037.
[42] R. Bakhshi-Jafarabadi, J. Sadeh, and M. Popov, "Maximum power point tracking injection method for islanding detection of grid-connected photovoltaic systems in microgrid," *IEEE Trans. Power Del.*, vol. 36, no. 1, pp. 168–179, Feb. 2021.
[43] A. S. Ahmed, "Investigation of wind characteristics and wind energy potential at Ras Ghareb, Egypt," *Renew. Sustain. Energy Rev.*, vol. 15, no. 6, pp. 2750–2755, Aug. 2011.
[44] C. B. Murugan, S. Natarajan, and R. Bensraj, "dSPACE based implementation of various inverted sine carrier PWM strategies for three phase five level H-bridge inverter," *Int. J. Adv. Eng. Technol.*, vol. 103, p. 112, Jan. 2016.
[45] Z. A. Ghani, M. A. Hannan, and A. Mohamed, "Renewable energy inverter development using dSPACE DS1104 controller board," in *Proc. IEEE Int. Conf. Power Energy*, Nov. 2010, pp. 69–73.

BASEM E. ELNAGHI received the B.Sc., M.Sc., and Ph.D. degrees in electrical power engineering from Suez Canal University, Port Said, Egypt, in 2002, 2009, and 2015, respectively. Since 2015, he has been an Associate Professor with the Electrical Engineering Department, Faculty of Engineering, Suez Canal University. He joined the Department of Faculty of Engineering, Suez Canal University, Rabigh. His research interests include AC and DC drives, direct torque and field-oriented control techniques, DSP control, control of electrical machines and wind energy conversion systems, and power electronics applications.

M. N. ABELWHAB received the B.Sc. degree from Zagazig University, and the M.Sc. and Ph.D. degrees from Mansoura University. He was a Superintended Engineer with the Naval Medical Research Unit Three (NAMRU-3), Cairo, then he participated in upgrading the electrical network of Abu Hamad Air Base, as an External Electrical Officer Engineer, and then he moved to Egyptian Electricity Transmission Company (EETC), as a Consultant Engineer. Eventually, he was appointed as an Assistant Professor (Teaching Staff Member) with the Electrical Engineering Department, Faculty of Engineering, Suez Canal University. He has published 30 papers in international journals and national and international conferences.

FATHY EL SAYED AHMED ABDEL-KADER received the B.Sc. degree in electrical power engineering from Mansoura University, in 1970, the M.Sc. degree in power and electric machinery from Helwan University, in 1977, and the Ph.D. degree in power and electric machinery, in 1979. Since 1989, he has been a Professor with the Electrical Engineering Department, Faculty of Engineering, Minoufiya University, Shebeen El-Kom. He has published over 120 papers, supervised over 50 M.Sc. and Ph.D. thesis, and examined over 70 M.Sc. and Ph.D. thesis. He is a Consultant of electrical machines.

AHMED M. ISMAIEL was born in September 1996. He received the B.Sc. and M.Sc. degrees from the Faculty of Engineering, Suez Canal University, Ismailia, Egypt, in 2019 and 2021, respectively. He is currently an Assistant Lecturer with the Electrical Power and Machine Engineering Department, Suez Canal University. His research interests include automation control, renewable energy, motor drive design and vector control techniques, and DSP control and power electronics applications.

REHAM H. MOHAMMED was born in March 1983. She received the B.Sc. and M.Sc. degrees from the Faculty of Engineering, Mansoura University, Egypt, in 2005 and 2010, respectively, and the Ph.D. degree from the Faculty of Engineering, Suez Canal University, Egypt, in 2016. In 2005, she joined the Faculty of Engineering, Mansoura University, as an Assistant Researcher. In 2011, she was an Assistant Lecturer with the Faculty of Engineering, Suez Canal University, where she is currently a Lecturer. She has more than 16 scientific research articles published in prestigious international journals.

MOHAMED E. DESSOUKI was born in Bohiera, Egypt, in 1976. He received the B.Sc., M.Sc., and Ph.D. degrees in electrical engineering from the Faculty of Engineering, Suez Canal University, in 1999, 2004, and 2010, respectively. He joined the Department of Electrical Engineering, Faculty of Engineering, Suez Canal University, as a Demonstrator, in 2000. Then, he became an Assistant Lecturer, from 2004 to 2010, and has been a Lecturer, since 2010. He joined the Department of Electrical Engineering, King Abdulaziz University, Rabigh. His research interests include AC and DC drives, direct torque and field-oriented control techniques, and DSP control and power electronics applications.